International Journal of
INTELLIGENT SYSTEMS AND APPLICATIONS IN ENGINEERING
ISSN:2147-6799 www.ijisae.org Original Research Paper

Performance Investigation of SINS/Odometer/NHC using Sequential Integrated Measurements

Gurram Muralikrishna[1], G. Mallesham*[2], M. Kannan[3]

Submitted:14/03/2024 **Revised**: 29/04/2024 **Accepted**: 06/05/2024

Abstract: The Strap-down inertial navigation system (SINS) has got excellent short term accuracy and is widely used for several autonomous land vehicle applications. However, due to its dead-reckoning process, the errors in navigation solution accumulate exponentially as the time progresses. In order to mitigate these errors, the use of auxiliary sensors has been explored in the recent past. An attempt has been made in this manuscript to use vehicle-borne odometer as an aiding sensor to have improved navigational positioning accuracy in horizontal and vertical channels of SINS. Further, the odometer misalignment angles and its lever-arm parameters are considered as error state vectors and a 21-state extended Kalman filter (EKF) is devised. Pulse count per unit sample interval is pre-processed to generate velocity information in odometer sensor assembly frame and used as measurement along with non-holonomic constraints (NHC). The efficacy of the proposed method is investigated by sequential processing of the measurements through sequential version of EKF. Field trial results are presented and found to have improvement through incremental position as a measurement in odometer sensor frame with improved observability during estimation process of odometer scale factor and lever arm parameters. Further, the accuracy of estimated altitude along with horizontal position solution is demonstrated toward autonomous vehicle application with GNSS as a reference.

Keywords: *Accelerometer, Extended Kalman Filter, GPS, GNSS, Gyroscope, Kalman Filter, Inertial Navigation system, Odometer*

1. Introduction

Navigation system for intelligent autonomous land vehicle requires high position accuracy and is determined by grade of inertial sensors deployed in the field operations. The position and attitude accuracy of inertial navigation systems degrade over time. Hence, an external aiding is required to correct the errors in position, velocity and attitude vectors [1]. Odometer can be used as an aiding source of information, due to its self-contained operations and does not depend on external signal outages like in global navigation satellite systems (GNSS).

Inertial navigation system (INS) consists of 3 sets of gyroscope and accelerometer sensors, which are positioned orthogonal with respect to each other in order to sense the rotation and linear movements in 3 axes. Initial co-ordinates have to be provided to INS for providing real time navigation solution, i.e., position, velocity and attitude. INS works on the basic principle of dead-reckoning and provides the outputs, considering the previous known parameters and the present measurements from the inertial sensors. The time propagated errors in navigation system are inevitable and are dependent on grade of inertial sensors selected for SINS. As these errors increase with respect to time, it is highly desirable to develop modern artificial intelligence based navigation schemes using inertial navigation data even in harsh and adverse environment for obtaining better navigation accuracies [2]. Hence, the researcher(s) are exploring alternative means of achieving precise positioning accuracy by employing several auxiliary sensors [3] along with SINS.

The GNSS is considered to be one of the auxiliary sensors for minimizing the errors in SINS operation for long duration navigation of land vehicles. However, the GNSS is very much compromised under adverse conditions due to interference problem [4]. Hence, the alternative sensors like magnetometer, light detection and ranging (LiDAR), baro altimeter, wheel mounted odometer, Doppler velocity log (DVL), laser Doppler velocity (LDV) are explored to be one of the prominent auxiliary sensors for several practical applications[5]. Availability of all these sensors is not possible at a time in a vehicle of specific purpose. Hence, it is advised to consider only the economically viable sensor as space and size constraints are dominant. However, land vehicles are equipped with few of the above sensors and often odometer as a mandatory sensor due to high reliability and zero maintenance. A multi-sensor-data-fusion [6] which is emerging as one of the state of art technology, enables the combination of measurements of either one or more sensors in tandem with SINS and offers improved accuracy and availability to a greater level. The odometer along with baro altimeter data are considered together and explored the performance of SINS through tightly coupled (TC) scheme and loosely coupled (LC) schemes under GNSS compromised environment in [5]. The velocity

[1] *Research Scientist, Research Centre Imarat, Hyderabad, PIN 500069 ORCID ID: 0009-0007-7458-8571, mkgurram@gmail.com*
[2] *Professor, University College of Engineering, Dept of EE, Osmania University, Hyderabad. ORCID ID: 0009-0006-0004-4689, drgm@osmania.ac.in*
[3] *Senior Scientist, Research Centre Imarat, Hyderabad, PIN 500069 ORCID ID: 0009-0003-1178-0604, kannan.m.rci@gov.in*

information is well generated through an in-built point cloud feature of LiDAR and demonstrated for integral operation of SINS in [7]. However, the velocity information extracted shall be noisy due to environmental effects and tuning of such filter shall be tedious. An improved state transition matrix which is derived from error frame definition is devised in [8] at the cost of additional computations in real-time embedded processor of land navigation system. An evaluation function is well proposed based on norm of innovation vector in [9] which is further used along with EKF process.

A non-holonomic constraint (NHC) superimposed on the lateral and vertical axes of vehicle motion in a first along with odometer velocity is proposed in [10] and demonstrated an improved performance for low grade sensors/ODO integrated system. The observability analysis is well considered for estimability of odometer installation parameters like mis-alignment angles and scale factor in [11]. The mathematical model for vehicle steering motion along with ODO/NHC based measurements are considered for wheeled robots in [12]. The concept of a dual measurement model of odometer equipped on front and rear wheels is considered in [13].

The authors in [14] proposed s-domain analysis of inherent Schuler oscillations involved in SINS mechanization. The suitable damping scheme through steady state stability analysis as presented is found to be attractive but the tuning of feedback gains is limited over wide range of odometer measurements with high noise emanating from harsh environments. The authors in [15] presented the details of wheel mounted SINS mechanism and proposed different methods of integration of odometer data. However, MEMS based SINS with low accuracy are suitable for wheel mounting. But, the mounting of navigation grade SINS on a rotating wheel is bulky and often not suitable for high grade ring-laser gyroscopes and quartz accelerometers. Also, the achieved accuracies of less than 2% is limited as compared to the requirements of 1%. The wheel mounted SINS does communicate with on-board diagnostic (OBD-II) equipment with Bluetooth communication and often limited by real time delays. Measurements from virtual MEMS based INS are framed through independent measurements from the set of inertial sensors [16]. These measurements are pre-processed and a virtual centripetal acceleration along with NHC are considered for estimation process. However, the availability of several such measurements are limited due to size and space limitations in real-time applications. Also, the method is encouraging, but it is limited by its computational burden and low accuracy. Image processing techniques are used to extract the location information from Kilo meter sign boards in [17] and fused with SINS data through optimal state estimation. The authors presented that the proposed technique has got superior performance as compared to SINS/Odometer based solution. However, the Kilo meter sign boards are not available in all the road ways and need periodic update of the data base for effective photogrammetry along with tedious field-calibration process.

The observability analysis on integral operation of SINS with LDV is well presented by authors in [18] and demonstrated the superior performance of integrated operation of SINS/LDV. However, the LDV measurements are found to be influenced by environmental conditions. Often, such measurements are found to be noisy due to rainy conditions and dust deposition on its optical parts. The authors in [19] proposed to have NHC and considered the centripetal acceleration as an additional measurement in addition to forward velocity measurement from odometer. The authors presented the results for short duration navigation applications. However, the extension of such study is not explored for long duration operation. The method shall make use of IIR Butterworth filter to pre-process the accelerometer measurements. The concept of Schmidt KF based filter gain for integral operation of SINS/ODO/DVL is proposed in [20] for long distance navigation of land vehicle system. Also, the authors proposed to minimize the vertical channel error over its trajectory path. Though the results are promising, the information on odometer and DVL calibration parameters along with SINS sensor biases are found to be limited. Triangulation based ultra-wide band (UWB) sensors along with SINS/ODO have been used for unmanned vehicle navigation in coal mines [21]. But, the use of UWB sensors has got major problem with multi-reflections of signals and interfering with each other resulting in poorer positioning results. However, the authors tried to demonstrate that the integrated operation with UWB and Odometer has got improved accuracy and reliability for short distance coal mine applications. The intermittency of odometer and Doppler radar measurements are studied towards continued and integrated navigation solution in [22]. Both simulation and experimental study confirmed that the continuity of navigation information can be maintained under GNSS compromised environments. However, the apportioning of error budget in standalone operation of each auxiliary sensors and integrated operations were not listed out. The odometer measurements are used to damp out the local error growth in horizontal channels of SINS during GNSS degraded conditions [23]. The work proposed was to provide the continuous position information for autonomous vehicle applications.

Adaptive Kalman filtering (AKF) technique is employed in [24] to filter out the incoming noise from DVL measurements towards improving positioning accuracy of vessels. The AKF has been extended to be adaptive two-stage Kalman filter (ATKF) in [25] for improving the positioning accuracy of SINS/Odometer based integrated land navigation system. Also, the authors presented several

conditions of side slip, wheel skid and wheel slip for velocity measurement from wheel-mounted odometer. Fault detection and isolation based on χ^2 distribution is well presented in [26] for SINS/ODO based integrated navigation system.

Though several sensors are explored as the best auxiliary sensors along with fusion schemes, each one has got its own limitations. The authors in the present manuscript prefer to work with a self-contained odometer as one of the reliable source of forward velocity measurement. The odometer equipped with twin inductive sensing elements are considered to have long life with zero maintenance. However, the major problem with vehicle mounted odometer is its scale factor variation due to wear and tear of vehicle tyre. Hence, the authors in present manuscript prefer to estimate the odometer scale factor and other installation parameters like mis-alignment angles, and lever-arm parameters. Further, based on the limitations of works published in recent past, the authors in the present manuscript proposed to make use of integrated measurements of wheel-mounted odometer in body frame of sensor assembly rather than the pulse velocity as measurements. Further, NHC based measurements are superimposed to have the hybrid navigation solution along with wheel mounted odometer as an auxiliary sensor. The motivation for the present work is to demonstrate high accurate and high reliable integrated navigation mechanization through estimation of odometer installation parameters as well as estimation of SINS sensor bias vectors. The odometers measurements are processed to be integrated velocity over filter update cycle rather than the pulse-velocity model. Field experiments are carried out to demonstrate the efficacy of proposed method under GNSS-degraded environments for navigation of land vehicles.

The main contributions of this manuscript is:

a) Formulation of odometer measurement model with integrated velocity as measurements,

b) Integrated velocity vector NHC constraints over filter update cycle

c) Sequential processing of measurements using scalar EKF,

d) Covariance propagation with experimental data,

e) Validation of estimated bias vectors of inertial sensors through proposed integrated fusion scheme.

f) Comparing the performance of proposed Hybrid navigation scheme with GNSS and pure inertial navigation scheme.

The rest of the contents of the manuscript is presented as follows: In section 2, the details of SINS error model is presented. Section 3 presents about the measurement error model of odometer assembly to estimate the corresponding installation parameters. Section 4 presents the sequential EKF scheme along with consideration for propagation of error covariance P_k matrix. Section 5 presents the Field trial results along with discussion. Finally, the conclusion and scope of further improvements are presented in section 6.

1.1. Abbreviations and Acronyms

The following are the list of abbreviations followed the in the technical content of the manuscript:

DT - Distance Travelled

EKF - Extended Kalman filter

GNSS - Global navigation satellite system

HYBRID - Hybrid navigation (INS+ODO)

INS - Inertial navigation

KF - Kalman filter

NHC - Non-holonomic constraints

ODO - Odometer sensor assembly

PF - Particle filter

PSD - Power spectral density

RLG - Ring laser gyroscope

SINS - Strapdown inertial navigation system

UKF - Uncented Kalman filter

2. LINEAR ERROR MODEL OF INERTIAL NAVIGATION SYSTEM

The pictorial representation of autonomous vehicle equipped with SINS, Odometer and GNSS antenna is shown in Fig. 1. The SINS body frame, denoted by b-frame and is rigidly mounted on to the vehicle with the x_b -axis directing forward, the y_b -axis pointing right, and the z_b -axis downward. It is assumed that the SINS body is aligned with the vehicle v-frame with axes definition same as b-frame and any mis-alignment between these two frames shall be absorbed as bore-sight angles and is not considered in the present manuscript. The GNSS antenna which is used for reference positioning system is installed on roof top of mobile van. The odometer sensor assembly is mounted on rear wheel of vehicle as shown Fig. 1. The odometer sensor frame is denoted by odo-frame, and is defined at the measuring center of the non-steering wheel axis. The set of axes x_{odo}, y_{odo} and z_{odo} shows the forward, right and downward directions respectively.

2.1. Mechanization of SINS kinematic model

The basic concept of strap-down inertial navigation is propagation of the kinematic equations in north-east-down reference frame of SINS. Hence the basic equations are considered for the derivation of error mechanization in the

geo-detic frame of SINS. The superscript 'l' denotes the local level frame of navigation in local geo-detic frame with the position vector

$$P^l = \left[\phi_p, \Theta_p, h_p\right]^T$$

with ϕ_p as geo-detic latitude, Θ_p as geo-detic longitude, h_p- as

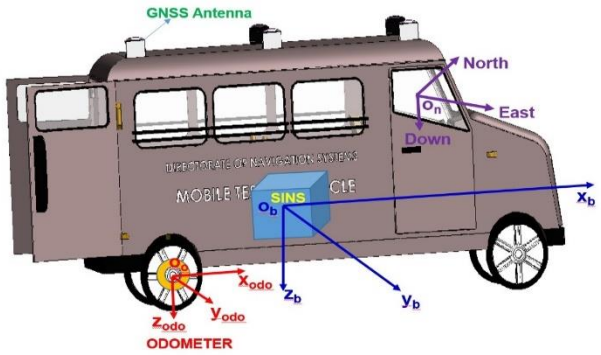

Fig.1. Pictorial representation of autonomous vehicle equipped with navigation sensors

height above ellipsoid as per WGS84 model. Similarly, the vector V^l represents the north-east-down components of velocity vector and defined as $V^l = \left[V_n^l, V_e^l, V_d^l\right]^T$. The principle of inertial navigation mechanization is presented in Fig.2.

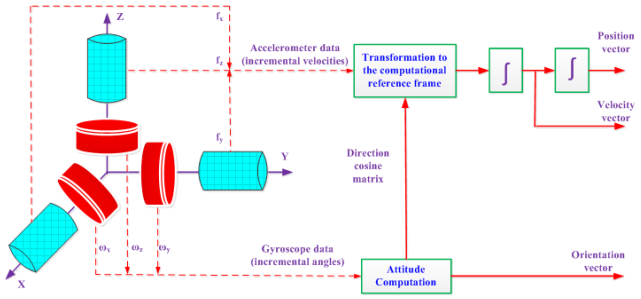

Fig.2 Principle of inertial navigation mechanization

The details of position, velocity and angles propagation models are presented as follows:

Position propagation model:

The geodetic position of vehicle in north-east-down frame of reference is expressed through propagation equation as:

Latitude propagation is given by:

$$\left[\dot{\phi}_p\right] = \frac{1}{r_{np}}\left[V_n^l\right] \tag{1}$$

Longitude propagation is given by:

$$\left[\dot{\Theta}_p\right] = \frac{1}{\cos(\phi_p)(r_{mp})}\left[V_e^l\right] \tag{2}$$

Altitude propagation is given by:

$$\left[\dot{h}_p\right] = -\left[V_d^l\right] \tag{3}$$

where $r_{np} = r_n + h_p$ and $r_{mp} = r_m + h_p$;

r_n - the normal radius and r_m - meditorial radius.

Velocity propagation model:

The dynamic model which represents the velocity propagation of SINS in local l-frame (i.e north-east-down frame) of reference is expressed as:

$$\begin{bmatrix}\dot{V}_n^l \\ \dot{V}_e^l \\ \dot{V}_d^l\end{bmatrix} = \begin{bmatrix}f_n \\ f_e \\ f_d\end{bmatrix} + g^l - \left[(w_{el}^l + 2w_{ie}^l)\right] \times \begin{bmatrix}V_n^l \\ V_e^l \\ V_d^l\end{bmatrix} \tag{4}$$

Where

$$(w_{el}^l + 2w_{ie}^l) = \begin{bmatrix}(\dot{\Theta}_p)\cos(\phi_p) + 2w_n^l \\ -\dot{\phi}_p \\ -(\dot{\Theta}_p)\sin(\phi_p) + 2w_d^l\end{bmatrix} \tag{5}$$

w_{ie}^l is the Earth rate vector computed in (l)-frame; w_{el}^l is the Earth transport rate expressed in (l)-frame and computed with reference to Earth fixed frame;

The measured specific acceleration vector is given by

$$f^l = \left[f_n^l \;\; f_e^l \;\; f_d^l\right]^T = C_l^b f^b \tag{6}$$

The transport rate vector expressed in l-frame as:

$$\left[w_{el}^l\right] = \left[\dot{\Theta}_p cos(\phi_p) \;\; -\dot{\phi}_p \;\; -\dot{\Theta}_p sin(\phi_p)\right]^T \tag{7}$$

The Earth rate vector expressed in l-frame as:

$$\left[w_{ie}^l\right] = \left[w_n^l \;\; 0 \;\; w_d^l\right]^T \tag{8}$$

The propagation of direction cosine matrix C_b^l which transforms a vector from local navigation frame, (l)-frame to SINS (b)- frame is computed by integration of

$$\dot{C}_b^l = C_b^l(\Omega_{ib}^b - \Omega_{il}^b) \tag{9}$$

where $\Omega = [\omega\times]$. ω_{ib}^{b} is the body rate vector measured in SINS (b)- frame; and ω_{il}^{b} is the body rate vector from inertial frame to (l)-frame and measured in SINS (b)-frame. The superscript 'l' denotes the local navigation frame; 'e' represents the earth-centered earth-fixed frame; 'b' represents the body frame, and 'i'denotes the earth-centered inertial frame; w_n is north component of Earth rate vector Ω_{ie} and is expressed as $w_n = \Omega_{ie} cos(\phi_p)$; w_d is down component of Earth rate vector Ω_{ie} and is expressed as $w_d = -\Omega_{ie} sin(\phi_p)$. g^l is the gravity vector; f^l is the specific force vector measured by accelerometers expressed in (l)-frame as $f^l = C_l^b f^b$; C_l^b is the direction cosine matrix which transforms the b-frame measured vector to (l)-frame. f^b is the specific force vector measured by accelerometers in SINS body frame; g_d^l is the gravity vector in (l)-frame.

2.2. Linearized Error State Dynamic model of SINS

Navigation error arises due to error in initial condition followed by the integration of instrumentation errors through the integration process. This section focuses on development of state space model for the navigation error vectors through the (l)-frame mechanization approach as defined in previous section 2.1. The concept of small signal error model is adapted for the position error propagation model. Let $\Delta P^l = \begin{bmatrix} \Delta\phi_p & \Delta\Theta_p & \Delta h_p \end{bmatrix}^T$ denotes the position errors of the INS, including the latitude error $\Delta\phi_p$, the longitude error $\Delta\Theta_p$, and the height error Δh_p. Through partial derivatives, the propagation of position error vector $\Delta\dot{P}_e^l = \begin{bmatrix} \Delta\dot{\phi}_p & \Delta\dot{\Theta}_p & \Delta\dot{h}_p \end{bmatrix}$ may be expressed as:

$$\left[\Delta\dot{P}^l\right] = \left[\Gamma_{PP}\right]\Delta P^l + \left[\Gamma_{PV}\right]\Delta V^l + \left[\Gamma_{PA}\right]\Delta A^l \quad (10)$$

where the error sensitivity matrix $[\Gamma_{PP}]$ which represent the position error propagation model may be written as:

$$\begin{bmatrix} \Delta\dot{\phi}_p \\ \Delta\dot{\Theta}_p \\ \Delta\dot{h}_p \end{bmatrix} = \left[\Gamma_{PP}\right]\begin{bmatrix} \Delta\phi_p \\ \Delta\Theta_p \\ \Delta h_p \end{bmatrix} \quad (11)$$

As the height is independent parameter and there is no coupling with ϕ_p and Θ_p it may be written as:

$$\Delta\dot{h}_p = 0 \quad (12)$$

The error sensitivity matrix $[\Gamma_{PP}]$ is expressed as

$$[\Gamma_{PP}] = \begin{bmatrix} 0 & 0 & \frac{-V_n^l}{r_{np}^2} \\ \frac{sin\phi_p}{cos^2\phi_p}\left(\frac{V_e^l}{r_{mp}}\right) & 0 & \frac{sin\phi_p}{cos^2\phi_p}\left(\frac{-V_e^l}{r_{mp}^2}\right) \\ 0 & 0 & 0 \end{bmatrix} \quad (13)$$

Similarly, the partial derivatives of rate of change of position vector with reference to velocity error may be expressed as:

$$\begin{bmatrix} \Delta\dot{\phi}_p \\ \Delta\dot{\Theta}_p \\ \Delta\dot{h}_p \end{bmatrix} = \left[\Gamma_{PV}\right]\begin{bmatrix} \Delta V_n^l \\ \Delta V_e^l \\ \Delta V_d^l \end{bmatrix} \quad (14)$$

where the error sensitivity matrix Γ_{PV} is expressed as:

$$[\Gamma_{PV}] = \begin{bmatrix} \frac{1}{r_{np}} & 0 & 0 \\ 0 & \frac{1}{cos\phi_p(r_{mp})} & 0 \\ 0 & 0 & -1 \end{bmatrix} \quad (15)$$

The error sensitivity of rate of change of position vector with reference to inherent error in Euler angles in (l)-frame $\Delta A^l = \begin{bmatrix} \Delta A_n^l & \Delta A_e^l & \Delta A_d^l \end{bmatrix}^T$ may be expressed as:

$$\begin{bmatrix} \Delta\dot{\phi}_p \\ \Delta\dot{\Theta}_p \\ \Delta\dot{h}_p \end{bmatrix} = \left[\Gamma_{PA}\right]\begin{bmatrix} \Delta A_n^l \\ \Delta A_e^l \\ \Delta A_d^l \end{bmatrix} \quad (16)$$

where the Jacobian matrix Γ_{PA} is expressed as:

$$\Gamma_{PA} = 0 \quad (17)$$

By using (2) and applying small signal perturbation model, the velocity error propagation model may be written as :

$$\begin{aligned} \left[\Delta\dot{V}^l\right] = {} & \left[\Gamma_{VP}\right]\Delta P^l + \left[\Gamma_{VV}\right]\Delta V^l \\ & + \left[\Gamma_{VA}\right]\Delta A^l + \left[C_l^b\right]\Delta f^b \end{aligned} \quad (18)$$

Where

$$\Gamma_{VP} = \begin{bmatrix} \Gamma_{VP(1)} & | & 0 & | & \Gamma_{VP(3)} \end{bmatrix} \quad (19)$$

with corresponding column vectors as follows:

The first column of Γ_{VP} is expressed as:

$$\Gamma_{VP(1)} = \begin{bmatrix} -\dfrac{(V_e^l)^2 \sec^2(\phi_p)}{r_{mp}} - 2w_n^l V_n^l \\ \dfrac{V_n^l V_e^l}{r_{mp}} \sec^2(\phi_p) + 2(w_n^l V_n^l + w_d^l V_d^l) \\ -2w_d V_e \end{bmatrix} \quad (20)$$

The third column of Γ_{VP} is expressed as:

$$\Gamma_{VP(3)} = \begin{bmatrix} -\dfrac{V_n^l V_d^l}{r_{np}^2} + \dfrac{(V_e^l)^2 \sec^2(\phi_p)}{r_{mp}^2} \\ -\dfrac{V_e^l V_d^l}{r_{np}^2} - \dfrac{V_e^l V_n^l}{r_{mp}^2} \tan(\phi_p) \\ \dfrac{(V_e^l)^2}{r_{mp}^2} + \dfrac{V_n^2}{r_{np}^2} \end{bmatrix} \quad (21)$$

Similarly,

$$\Gamma_{VV} = \begin{bmatrix} \Gamma_{VV(1)} & \Gamma_{VV(2)} & \Gamma_{VV(3)} \end{bmatrix} \quad (22)$$

with its column vectors computed as follows:

The first column of Γ_{VV} is expressed as:

$$\Gamma_{VV(1)} = \begin{bmatrix} -\dfrac{V_d}{r_{np}} \\ -\dfrac{V_e^l}{r_{mp}} \tan(\phi_p) + 2(w_d) \\ 2(\dfrac{V_n^l}{r_{np}}) \end{bmatrix} \quad (23)$$

The second column of Γ_{VV} is expressed as:

$$\Gamma_{VV(2)} = \begin{bmatrix} \dfrac{2V_e^l}{r_{mp}} \tan(\phi_p) - 2w_d \\ -\dfrac{V_d^l}{r_{mp}} - \dfrac{V_n^l}{r_{mp}} \tan(\phi_p) \\ \dfrac{2V_e^l}{r_{mp}} + 2w_n \end{bmatrix} \quad (24)$$

The third column of Γ_{VV} is expressed as:

$$\Gamma_{VV(3)} = \begin{bmatrix} -\dfrac{V_n^l}{r_{np}} \\ -\dfrac{V_e^l}{r_{mp}} + 2(w_n) \\ 0 \end{bmatrix} \quad (25)$$

Finally, the error velocity Jacobian with respective to mis-alignment angles is calculated as:

$$\Gamma_{VA} = \left[f^l \times \right] = \text{ Skewed matrix of vector } \left[f^l \right] \quad (26)$$

Mis-alignment angle propagation:

The body measured angular rate vector w^b may be transformed to (l)-frame as:

$$w^l = C_l^b w^b \quad (27)$$

Measured angular rate as shown in (27) may be perturbed through:

$$\left.\begin{aligned} \tilde{w}^l &= w^l + \Delta w^l \\ \tilde{w}^b &= w^b + \Delta w^b \\ \tilde{C}_b^l &= \left[I - \Delta A^l \right] C_b^l \end{aligned}\right\} \quad (28)$$

The propagation of direction cosine matrix C_b^l may be written as:

$$\dot{C}_b^l = \left[C_b^l \right] \left[w^b \times \right] - \left[w^l \times \right] \left[C_b^l \right] \quad (29)$$

By substituting (27) in (28) and (29), the small signal perturbed model for attitude error may be written as:

$$\Delta \dot{A}^l = -\left[w^l \times \right] \Delta A^l - \left[C_b^l \right] \Delta w^b + \Delta w^l \quad (30)$$

where $\left[w^l \times \right]$ is skew-symmetric matrix of w^l vector and is expressed as :

$$\left[w^l \times \right] = \begin{bmatrix} 0 & -w_d^l & w_e^l \\ w_d^l & 0 & -w_n^l \\ -w_e^l & w_n^l & 0 \end{bmatrix} \quad (31)$$

The Δw^l is the error in rotation rate of reference frame and may be expressed as partial derivatives of ΔP^l and ΔV^l as:

$$\Delta w^l = \left[\frac{\Delta w^l}{\Delta P^l} \right] \Delta P^l + \left[\frac{\Delta w^l}{\Delta V^l} \right] \Delta V^l \quad (32)$$

By using (31) , the (29) may be written as:

$$\begin{aligned} \left[\Delta \dot{A}^l \right] = &\left[\Gamma_{AP} \right] \Delta P^l + \left[\Gamma_{AV} \right] \Delta V^l \\ &+ \left[\Gamma_{AA} \right] \Delta A^l + \left[C_b^l \right] \Delta w^b \end{aligned} \quad (33)$$

Where

$$\Gamma_{AP} = \begin{bmatrix} w_d^l & 0 & -\frac{V_e^{l2}}{r_{md}^2} \\ 0 & 0 & \sec^2(\phi_p)(V_n / r_{np}^2) \\ -\frac{V_e^l \sec^2(\phi_p)}{r_{mp}} - 2w_n & 0 & \tan(\phi_p)(V_e^l / r_{mp}^2) \end{bmatrix} \quad (34)$$

$$\Gamma_{AV} = \begin{bmatrix} 0 & \frac{1}{r_{mp}} & 0 \\ -\frac{1}{r_{mp}} & 0 & 0 \\ 0 & -\frac{1}{r_{mp}}\tan(\phi_p) & 0 \end{bmatrix} \quad (35)$$

$$\Gamma_{AA} = \begin{bmatrix} 0 & -\frac{V_e^l tan(\phi_p)}{r_{mp}} + w_d^l & \frac{V_n}{r_{np}} \\ \frac{V_e^l tan(\phi_p)}{r_{mp}} - w_d^l & 0 & \frac{V_e^l}{r_{mp}} + w_n^l \\ -\frac{V_n}{r_{np}} & -\frac{V_e^l}{r_{mp}} - w_n^l & 0 \end{bmatrix} \quad (36)$$

The equations (10), (18), and (33) are combined together to represent a small signal mathematical model of SINS as:

$$\begin{bmatrix} \Delta \dot{P}^l \\ \Delta \dot{V}^l \\ \Delta \dot{A}^l \end{bmatrix} = \begin{bmatrix} \Gamma_{PP} & \Gamma_{PV} & \Gamma_{PA} \\ \Gamma_{VP} & \Gamma_{PV} & \Gamma_{VA} \\ \Gamma_{AP} & \Gamma_{AV} & \Gamma_{AA} \end{bmatrix} \begin{bmatrix} \Delta P^l \\ \Delta V^l \\ \Delta A^l \end{bmatrix} + \begin{bmatrix} 0 \\ C_b^l \Delta f^b \\ -C_b^l \Delta w^b \end{bmatrix} \quad (37)$$

2.3. Composite system matrix through augmentation of states

Inertial sensors for navigation systems have systematic errors and random errors. The systematic errors are measured through calibration process and compensated during navigation process. However, the modelling of random errors along with compensation is a challenging activity. These random errors are the inherent errors of inertial sensors within SINS system which will cause the drift in end-computed navigation state information. Hence, it is important to model them through state augmentation approach. However, there are several parameters to be consider as shown in Fig. 3 and only the bias parameters are considered in the present manuscript as a trade-off between increased accuracy and size of the filter. It is to be noted that the higher order terms like scale factor and non-linearity shall have better estimation strategy for high dynamic motion path and observability criteria and need not be considered for low-dynamic land vehicle applications. Hence, the lumped parameter models are assumed to represent the equivalent bias vectors of inertial sensors and are considered for the present work.

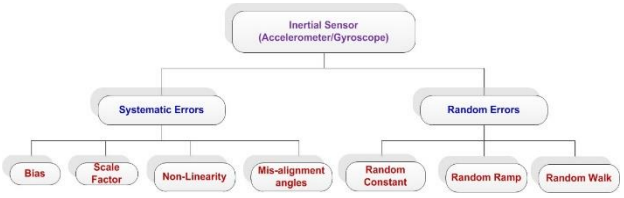

Fig. 3. Different types of errors of inertial sensors measurements.

Let Δf^b and Δw^b represent the error state vectors in specific force and angular rate measurements respectively. These measurement errors include both random noise terms and left over errors in calibration process. Given the measurements $\tilde{f}^b$ and $\tilde{w}^b$, the estimates of the bias vectors $\Delta\hat{f}^b$ and $\Delta\hat{w}^b$, the specific force and angular rate vectors towards the navigation computation are listed as:

$$f^b = \tilde{f}^b - \Delta\hat{f}^b \quad (38)$$

$$w^b = \tilde{w}^b - \Delta\hat{w}^b \quad (39)$$

Assuming Δf^b and Δw^b are the random constants of the accelerometer bias vector and gyro bias vector accordingly through lumped parameter model, the corresponding error propagation equations may be written as:

$$\Delta\dot{f}^b = 0 \quad (40)$$

$$\Delta\dot{w}^b = 0 \quad (41)$$

The error state equations derived from (10), (18), (33), (40), and (41) are put together and represented in state space form with $[\Delta x]$ as error state vector and finally represented in component form as:

$$[\Delta x_{INS}^l] = \begin{bmatrix} \Delta P^l & \Delta V^l & \Delta A^l & \Delta w^b & \Delta f^b \end{bmatrix}^T \quad (42)$$

and the corresponding small signal error model is expressed as

$$\begin{bmatrix} \Delta \dot{P}^l \\ \Delta \dot{V}^l \\ \Delta \dot{A}^l \\ \Delta \dot{w}^b \\ \Delta \dot{f}^b \end{bmatrix} = \begin{bmatrix} \Gamma_{PP} & \Gamma_{PV} & \Gamma_{PA} & 0 & 0 \\ \Gamma_{VP} & \Gamma_{PV} & \Gamma_{VA} & 0 & \Gamma_{Vf^b} \\ \Gamma_{AP} & \Gamma_{AV} & \Gamma_{AA} & \Gamma_{Aw^b} & 0 \\ 0 & 0 & 0 & 0 & 0 \\ 0 & 0 & 0 & 0 & 0 \end{bmatrix} \begin{bmatrix} \Delta P^l \\ \Delta V^l \\ \Delta A^l \\ \Delta w^b \\ \Delta f^b \end{bmatrix} \quad (43)$$

Where

$$\Gamma_{Vf^b} = -C_b^l \quad (44)$$

$$\Gamma_{Aw^b} = C_b^l \quad (45)$$

Equation (43) is represented in short form for the linear error dynamical model of INS in time domain form as:

$$\left[\Delta \dot{x}(t)\right]_{15\times1} = \left[\Gamma_{INS}\right]_{15\times15}\left[\Delta x(t)\right]_{15\times1} + w(t) \quad (46)$$

3. PROPOSED ODOMETER MESUREMENT MODEL

GNSS is considered to be a potential aiding source to the SINS to reduce the accumulation of errors for several applications. However, GNSS can be compromised and degraded in urban canyons, tunnels, and in the adverse territorial conditions. Alternatively, the odometer as a vehicle motion sensor is found to be a most suitable and cost-effective device that is immune to the several environment-related errors. The odometer can be used to minimize the accumulated INS errors as the time progresses. The odometer sensor assembly has got mechanical housing with phonic wheel and a set of high reliable inductive sensors. A phonic wheel is required with serrations to generate the pulse high and low output. The tooth of phonic wheel should be in the vicinity of sensing distance and the number of tooth required will be as per the resolution requirements of the distance travelled computation. Two inductive proximity sensors are used to differentiate the vehicle motion in forward and reverse motion by detecting the phase lead and phase lag from pulse output of both the sensors. Placement of proximity sensors near to phonic wheel should be arranged in such a manner that both sensor output pulses should be in quadrature phase shift. The stream of electrical pulses are sent to timer/counter of Processing electronics to generate the forward motion detection through its associated value of nominal scale factor.

3.1. Measurement model based on Odometer velocity vector

The required measurement towards the optimal state estimation through proposed Kalman filtering process can be constructed by the velocity differences between the b-frame of INS and odo-frame of Odometer sensor assembly. Let the odometer parameter be represented as:

V^{odo} - Forward velocity of vehicle along x-axis as measured by Odometer sensing assembly

SF^{odo} - Scale factor of odometer which converts the measured pulses per sample time to equivalent forward velocity

ΔSF^{odo} - The error in Scale factor of odometer measurement

ΔL^{odo} - Error in lever arm vector of odometer assembly from the installation location of SINS

M^{odo} - Mis-alignment angles from odometer assembly to b-frame of SINS

C_b^{odo} - Lever arm vector of odometer assembly from the installation location of SINS

The error sensitivity measurement model of odometer based on measured forward velocity V^{odo} on odometer sensor assembly frame is written as:

$$\begin{aligned}\Delta z^{odo} &= C_l^{odo}[\Delta V^l] + C_l^{odo}V^l \times [\Delta A^l] + \\ &\quad V^{odo} \times [M^{odo}] - C_b^{odo}[w^b \times \Delta L^{odo}] \\ &\quad - (\Delta SF^{odo})V^{odo}\end{aligned} \quad (47)$$

where C_l^{odo} represents the transformation matrix from odo-frame to l-frame and $M^{odo} = \begin{bmatrix} M_{yz}^{odo} \\ M_{xz}^{odo} \\ M_{xy}^{odo} \end{bmatrix}$ with

$$\begin{bmatrix} M_{yz}^{odo} \\ M_{xz}^{odo} \\ M_{xy}^{odo} \end{bmatrix} \mathrm{X} = \begin{bmatrix} 0 & -M_{xy}^{odo} & M_{xz}^{odo} \\ M_{xy}^{odo} & 0 & -M_{yz}^{odo} \\ -M_{xz}^{odo} & M_{yz}^{odo} & 0 \end{bmatrix} \quad (48)$$

And

$$V^{odo}\mathrm{X} = \begin{bmatrix} V_x^{odo} \\ V_y^{odo} \\ V_z^{odo} \end{bmatrix} \mathrm{X} = \begin{bmatrix} 0 & 0 & 0 \\ 0 & 0 & -V_x^{odo} \\ 0 & V_x^{odo} & 0 \end{bmatrix} \quad (49)$$

Where the mathematical symbol X represents the skewed symmetric matrix operation on vector. V^{odo} is a velocity vector defined in odometer sensor assembly frame with V_x^{odo} as incremental velocity as measured by odometer along x_{odo} axis. an V_y^{odo} and V_z^{odo} are the resultant velocity components with zero mean white noise and are due to non-holonomic constraints (NHC) imposed along the y_{odo}-axis and z_{odo}-axis respectively.

$$\begin{aligned}\Delta z^{odo} &= [C_b^{odo}C_l^b][\Delta V^l] \\ &\quad + \begin{bmatrix} 0 & 0 & 0 \\ 0 & 0 & -V_x^{odo} \\ 0 & V_x^{odo} & 0 \end{bmatrix}\left[M^{odo}\right] \\ &\quad - (\Delta SF^{odo})V^{odo} - C_b^{odo}[w_{eb}^b \times \Delta L^{odo}]\end{aligned} \quad (50)$$

Since M_{yz} is not observable it can be removed from state vector. By forcing the other two components V_y^{odo} and

V_z^{odo} to zero and rearranging the states $M_{xz}^{odo}, M_{xy}^{odo}$ and ΔSF^{odo}, the measurement equation required for the proposed Kalman filtering process is expressed as:

$$\Delta z^{odo} = [C_b^{odo} C_n^b][\Delta V^n] + \begin{bmatrix} -V_x^{odo} & 0 & 0 \\ 0 & 0 & -V_x^{odo} \\ 0 & V_x^{odo} & 0 \end{bmatrix} \begin{bmatrix} \Delta SF^{odo} \\ M_{xz}^{odo} \\ M_{xy}^{odo} \end{bmatrix} - C_b^{odo}[w_{ib}^b \times \Delta L^{odo}] \quad (51)$$

3.2. State-space model for Odometer velocity measurements

Once the SINS and Odometer are mounted on a vehicle, the relative mounting angles between the b-frame, and o-frame are fixed and to be measured. Also, the lever arm values between measurement centres of o_b and o_{odo} to be measured. Further, the scale factor of the odometer will be varying due to environmental conditions and is prone to tyre pressure variations. These parameters are conventionally measured through a dedicated calibration process by using standard level meters, guages, and a fixed track straight line motion. Since, this process is very cumbersome and having several constraints from the field operations, it is proposed to estimate the parameters though filtering process. The corresponding scale factor error, installation angles, and lever arm vector are considered as random constants and their error equations are expressed as:

$$\Delta \dot{SF}^{odo} = 0 \quad (52)$$

$$\dot{M}_{xy}^{odo} = 0 \quad (53)$$

$$\dot{M}_{xz}^{odo} = 0 \quad (54)$$

$$\Delta \dot{L}^{odo} = 0 \quad (55)$$

The equations (52), (53), (54), and (55) are arranged together through a composite linear dynamical equation and represented as

:

$$\Delta \dot{x}_{6\times1}^{odo} = 0 \quad (56)$$

where

$$\Delta x_{6\times1}^{odo} = \begin{bmatrix} \Delta \dot{SF}^{odo} & \Delta \dot{M}_{xy}^{odo} & \Delta \dot{M}_{xz}^{odo} & \Delta \dot{L}^{odo} \end{bmatrix} \quad (57)$$

Using (57) and (58), the measurement model of odometer may be expressed as:

$$\Delta z_k^{odo} = \left[\Delta h_k^{odo}\right] \Delta x_k^{odo} + \vartheta_k \quad (58)$$

Where

$$\left[\Delta h_k^{odo}\right] = \left[0\, \Delta h_{(v)}^{odo}\, 0\, 0\, 0 \quad \Delta h_{(SF,M)}^{odo}\, \Delta h_{(L)}^{odo}\right] \quad (59)$$

With

$$\left[\Delta h_{(v)}^{odo} =\right]\left[C_b^{odo} C_n^b\right] \quad (60)$$

$$\Delta h_{(SF,M)}^{odo} = \begin{bmatrix} -V_x^{odo} & 0 & 0 \\ 0 & 0 & -V_x^{odo} \\ 0 & V_x^{odo} & 0 \end{bmatrix} \quad (61)$$

$$\Delta h_{(L)}^{odo} = -C_b^{odo}[w_{ib}^b \times] \quad (62)$$

3.3. State-space model for Odometer integrated system

According to the error model of the proposed hybrid (INS/ODO) navigation as explained in previous section, the error state model of the INS/ODO integration can be constructed. The corresponding linear error dynamical model of SINS as shown in (43) and (57) with F_{HYBRID} as system matrix is represented in time domain form as:

$$\left[\Delta \dot{x}(t)\right]_{21\times1} = \left[\Gamma_{HYBRID}\right]_{21\times21} \left[\Delta x(t)\right]_{21\times1} + \xi(t) \quad (63)$$

Where

$$\left[\Gamma_{HYBRID}\right]_{21\times21} = \begin{bmatrix} \Gamma_{INS} & 0_{15X6} \\ 0_{6X15} & 0_{6X6} \end{bmatrix} \quad (64)$$

By framing $\Delta x(t)$ as a 21-dimensional error state

vector as:

$$\left[\Delta \dot{x}(t)\right]_{21\times1} = \left[\Delta x_{INS}^l \quad \Delta x^{odo}\right]^T \quad (65)$$

where ϕ_{INS} is a 15×15 state transition matrix based on the mathematical error model of INS as defined in (46).

The equation (63) is discretized for the sake of implementation of extended Kalman filter[27] as :

$$\Delta x_{k+1} = \phi_k \Delta x_k + \xi_k \quad (66)$$

where ξ_k is process noise matrix with all its components having Gaussian noise with mean zero as:

$E[\xi_k] = 0$ and $E[\xi_k \xi_j] = q_k \delta_{kj}$ where δ_{kj} assumes 1 for diagonal elements and zero for all other elements and the process noise matrix q_k is formulated by extracting the power-spectral density (PSD) parameters of gyroscopes and accelerometers respectively.

4. SEQUENTIAL PROCESSING OF ODOMETER MESUREMENTS THROUGH EKF

4.1. Error state estimation through Extended Kalman filter

This section provides the system-error models and measurement updating models of the loosely-coupled

navigation of INS/odometer based on an extended Kalman filter (EKF). Since, the authors in the present manuscript devised the mathematical models for high accuracy accelerometers and ring laser gyroscopes (RLG) with less bias error, the extended Kalman filter has been considered with relatively less number of computations. Hence, the derived SINS linearized models as presented in previous section shall be the basis for the implementation of EKF based estimation [28].

The sensor measurements of SINS are propagated through non-linear equations and the corresponding small signal perturbed model is derived with an aim of devising error state estimator through Extended Kalman filter. However, there are other non-linear filtering methods available in the published works. The unscented Kalman filter (UKF) is widely used for MEMS based SINS applications for commercially ground vehicles where the dependency on GNSS is high [29]. Similarly, particle filter (PF) is devised and highly recommended for MEMS based SINS which has the high level of non-linearity between the two epochs of filter update interval. The works reported in [30-31] have confirmed that the EKF and UKF processes are mathematically equivalent with first one has got simpler mathematical operations compared to second one.

The extended Kalman filtering is formulated as:

EKF based measurement update scheme:

The Kalman gain is computed as:

$$k_k = p_{k+1}^{(-)} h_k^T [r_k + h_k p_{k+1}^{(-)} h_k^T]^{-1} \quad (67)$$

$$\Delta x_{k+1}^{(+)} = \Delta x_{k+1}^{(-)} + k_k [residual]_k \quad (68)$$

$$p_{k+1}^{(+)} = u_k p_{k+1}^{(-)} u_k^T + k_k r_k k_k^T \quad (69)$$

Where

$$u_k = I - k_k h_k \quad (70)$$

The error residual vector $residual_k$ is computed as:

$$[residual]_k = \left[\Delta z^{odo}\right]_k - [h_k] \Delta x_{k+1}^{(-)} \quad (71)$$

EKF based time update scheme:

$$\Delta x_{k+1}^{(-)} = \Phi_k \Delta x_k^{(+)} \quad (72)$$

$$p_{k+1}^{(-)} = \Phi_k p_k^{(+)} \Phi_k^T + q_k \quad (73)$$

Since, the Kalman gain k_k has to deal with inversion of diagonalized version of measurement covariance matrix, there is a likely chance that the denominator may approach close to zero. This leads to the divide by zero problem in an embedded computer leading to the soft failure of SINS. Hence, the batch processing technique of Kalman gain is re-formulated as scalar processing of EKF where the measurements are sequentially processed one after the other one. The measurement matrix r_k is assumed to be diagonal as :

$$r_k = \mathrm{diag}\left[r_{k_{(1)}}, r_{k_{(2)}}, r_{k_{(3)}} \right] \quad (74)$$

Where `diag' represents the diagonalal elements of matrix r_k of size 3×3. In order to have sequential processing, the corresponding measurement equation is written as:

$$\Delta \hat{z}_{(k)(j=1,2,3)} = \left[h_{k,((j=1,2,3))} \right] \Delta \hat{x}_k + \vartheta_{k,j=1,2,3} \quad (75)$$

Sequential Kalman filter execution :

Stage 1: Initialize the sequential EKF parameters as:

$$\Delta x_0^{(+)} = E[\Delta x_0] = 0 \quad (76)$$

$$p_0^{(+)} = E[(\Delta x_0 - \Delta x_0^{(+)})(\Delta x_0 - \Delta x_0^{(+)})^T] \quad (77)$$

$$r_k = \mathrm{diag}(r_{k,(1)}, r_{k,(2)}, \ldots, r_{k,(3)}) \quad (78)$$

Stage 2: Compute error covariance matrix at each time step k as shown in (73) and the associated the process noise covariance matrix q_k based on PSD values of inertial sensors.

Stage 3: Initialize the error estimate of state vector and its associate error covariance matrix as : $\left[\Delta x_{k,(0)}^{(+)} = \Delta x_k^{(+)}\right]$ and $\left[p_{k,(0)}^{(+)} = p_0^{(-)}\right]$ and the update the measurement equations at each time step k as follows:

(a) Considering the one measurement at a time from error residual vector $[residual]_{3\times1}$ the following computations are performed sequentially for $i = 1, 2, 3$

(b) Re-assign the a posteriori estimate of error state vector and its covariance as:

$$\Delta x_{k+1}^{(+)} = \Delta x_{k,(i)}^{(+)} \quad (79)$$

$$p_{k+1}^{(+)} = p_{k,(i)}^{(+)} \quad (80)$$

Stage 4: After processing three measurements, the EKF corrections are generated and are applied to the plant model through $\Delta x_{k+1}^{(+)}$ at the $(k+1)^{th}$ instance.

5. FIELD EXPERIMENTAL RESULTS

The strap-down inertial navigation mechanization in local tangent plane is implemented in embedded system-on-chip

(SOC) processor of SINS. The incremental angles and incremental velocities from inertial sensor module are sampled at 400 Hz. The attitude information is derived at every 10 milli seconds. Further, Simpson's numerical integration is performed at every 20 milli seconds for velocity and position computations. To test the algorithmic performance of proposed scheme, a phonic wheel equipped with two inductive sensors of make from M/s SICK are realized and mounted on non-steering wheel of the vehicle as shown in Fig.5. Inertial navigation system with the required algorithmic implementation in its software module and equipped with in-built GNSS receiver is installed in the mobile van test facility. The experiments are conducted by keeping a navigation grade ring laser gyro (RLG)-based high accuracy sensor cluster statically for one hour. The studies have been carried by considering the nominal errors values of inertial sensors: 70 micro g bias error on accelerometer measurement and 0.03 deg/hour drift error on gyroscope measurement. The detailed specifications of the SINS is shown in Table. 1

Table 1. Typical errors of inertial sensors of SINS under field evaluation

Sensor: Accelerometer	**Parameter**
Bias repeatability	70 μg, 1 σ
Scale factor Accuracy	50 ppm, 1 σ
Random Walk	10 μg/ √(hour)
Sensor: Gyroscope	**Parameter**
Bias repeatability	0.03 deg/hour, 1 σ
Scale factor Accuracy	50 ppm, 1 σ
Random Walk	0.01 deg/√(hour)

Van trial test is carried out to validate position accuracy of proposed hybrid navigation solution (INS+ODO) with respect to GNSS under dynamic motion conditions. The following are the two conditions considered:

1) Pure inertial mode where no external aiding is used: Position error for 1 hour operation
2) Hybrid navigation in which inertial sensor data is fused with odometer data over 15km of travelled distance.

5.1. Static testing over 1 hour duration

The navigation test is run for 3600 sec. The results are plotted and analyzed against the standard specifications of 1.0 NM/hour (1σ) for the sensor specifications listed out in Table1. Further, the GNSS Receiver (GPS) computed positions and velocities in (l)-frame are taken as reference. Finally, the optimally fused data of pure inertial navigation solution with Odometer measurements are studied and plotted. Initially the static navigation runs are given for different set of random values of sensor error as specified in Table 1 and errors of 12 runs are shown in the Fig.4 and Fig.5 for position errors and velocity errors respectively. These errors are found to be oscillatory with a Schuler oscillating frequency of 84.4 minutes. These errors represent the type of errors involved in position and velocity vectors as the time progresses and justifies the need of proposed multi-sensor data fusion by using Odometer or GNSS as an auxiliary sensor for accurate positioning the vehicle.

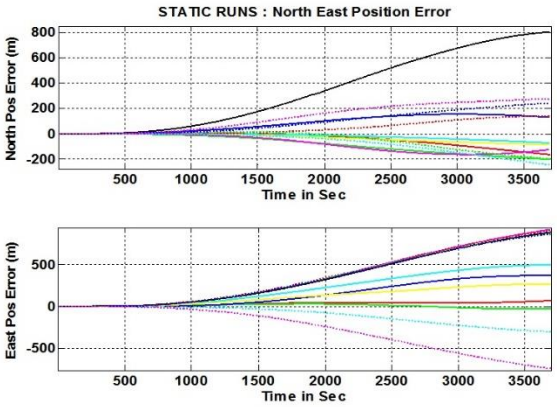

Fig. 4. Navigational position error drift for 12 independent runs with each one for 1 hour duration

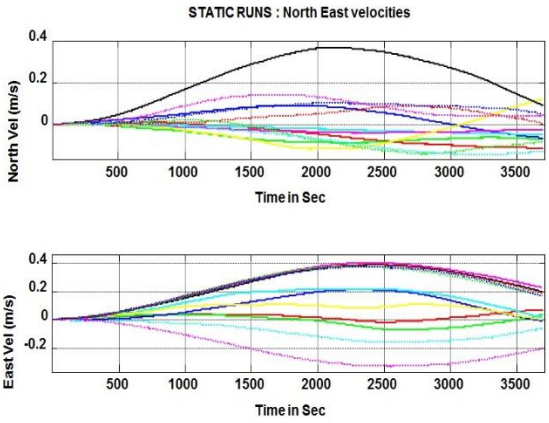

Fig. 5. Navigational velocity error drift for 12 independent runs with each one for 1 hour duration

5.2. Dynamic tests with odometer sensor integrated with SINS

GNSS provides position-velocity-time information with bounded errors irrespective of time of operation. Under benign conditions, it is always preferred to fuse the pure INS data with GNSS data to generate the accurate navigation solution. However, the GNSS being as an external system, it has its own limitations regarding the signal reception and its associated signal processing.

During the GNSS denied conditions like when the vehicle is moving in urban canyons or thick vegetation, the GNSS suffers from loss of signal reception and hence, the navigation solution will start drifting towards pure inertial navigation mode. In order to damp these errors, it is planned to use Odometer data from odometer sensor mounted on axle wheel of autonomous vehicle which provides the forward velocity of the vehicle. The test setup with in-house built SINS, Odometer assembly, and GNSS antenna are shown in Fig. 6.

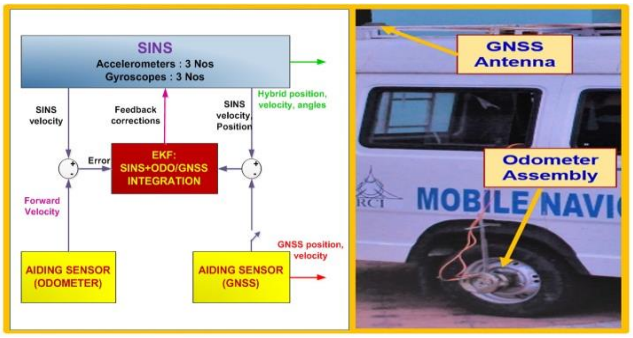

Fig. 6. Mobile navigation test facility with SINS, Odometer assembly and GNSS antenna on the roof top of mobile van.

The additional 6 states are introduced to cater the uncalibrated odometer parameters and total 21-State Extended Kalman filter is designed to get the optimal navigation solution. The error states are tabulated in Table. 2.

Table 2. States of 21-State Extended Kalman Filter (INS+GPS+ODO)

S.No	Vector Name	Number of states
1	Position	3 (Latitude, Longitude, Height)
2	Velocity	3 (V_n^l, V_e^l, V_d^l)
3	Attitude	3 (ψ, θ, ϕ)
4	Gyroscope Bias	3 $(\Delta w^b{}_x, \Delta w^b{}_y, \Delta w^b{}_z)$
5	Accelerometer Bias	3 $(\Delta f^b{}_x, \Delta f^b{}_y, \Delta f^b{}_z)$
6	Odometer Scale Factor, Pitch & Azimuth Misalignment	3 $(SF^{odo}, M_{xz}^{odo}, M_{xy}^{odo})$
7	Odometer Lever Arms	3 $(L_x^{odo}, L_y^{odo}, L_z^{odo})$

The duration of test is considered for 3500 sec. The results are plotted and analyzed against the standard specifications. Also, the GNSS receiver computed positions and velocities in (l)-frame are taken as reference. Finally, the optimally fused data of pure inertial navigation solution with odometer measurements are studied and plotted under the label HYBRID (INS+ODO). The colour codes defined for interpretation of results are shown in Table 3.

Table 3. Colour Codes for Data Interpretation for Fig. 8 to Fig.11

Color Code	Label Name	Description
Blue	INS	Pure inertial navigation solution based on inertial sensor(with vertical channel damping
Red	GNSS	GNSS Reference navigation solution based on satellite position Fix
Green	HYBRID (INS+ODO+NHC)	Pure Inertial + Odometer fused hybrid navigation solution + non-holonomic constraint (NHC)

The pure INS, hybrid computed positions (HYBRID) along with GNSS measured positions are plotted in Fig.7. It is found that the pure INS computed position profile is drifted from the GNSS position profile whereas the hybrid scheme computed position profile is matched closely with GNSS computed position profile. Further, in order to quantify the amount of errors the error in positions with reference to time is plotted in Fig. 8. It is found that the pure INS has shown 1.8 Km and 1.2 Km position errors in north and east channels respectively. The height error in pure and hybrid channels are found to be within 20 meters. The error in height computed by pure INS is damped out by external baro altimeter data whereas the height computed by proposed hybrid scheme with odometer as an auxiliary sensor is shown similar performance within 20 meters and 45 meters for north and east channels as shown in Fig. 9. This is a significant achievement and the need of baro-altimeter does not exists as long the proposed hybrid navigation scheme is active. The hybrid computed horizontal position errors are shown in Fig. 8 and found to be 20 meters and 50 meters for north and east channels respectively at 3500 sec.

The Euler angle profile of the SINS during the motion is presented in Fig. 10. The van has moved along the road covering 3 Mini Mountains indicated the pitch-up and pitch down conditions. The efficiency of height calculation can be better judged during the motion path at different elevated

track conditions. Hence from Fig. 9, it can be concluded that the height errors are well within 20 meters accuracy under varying altitude profile along the motion path.

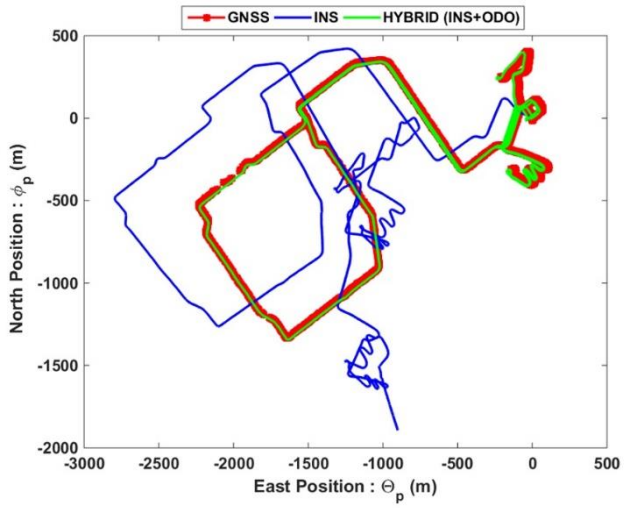

Fig. 7. North and East position pure INS, GNSS and proposed Hybrid (INS+ODO) navigation mechanization

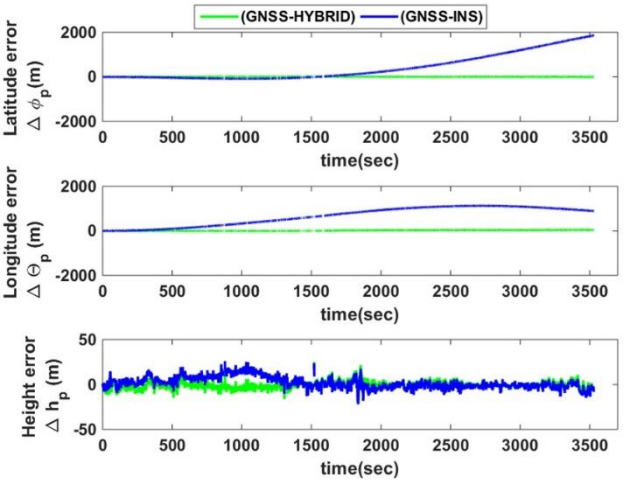

Fig. 8. North and East position errors of pure INS and proposed Hybrid (INS+ODO) navigation mechanization

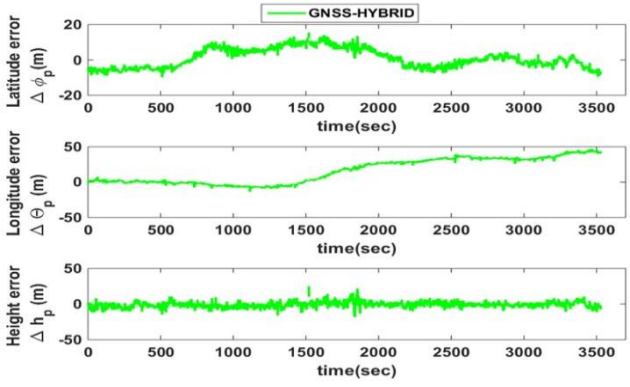

Fig. 9. North and East position errors of proposed Hybrid (INS+ODO) navigation mechanization

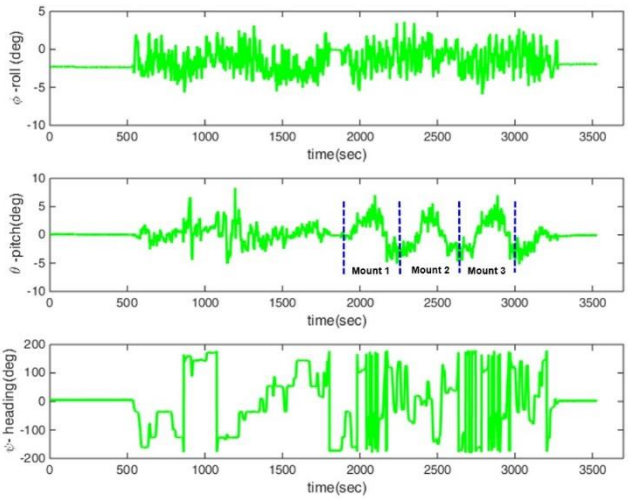

Fig. 10. Euler angles of vehicle during motion testing

The velocity profile of the van as recorded by pure INS, hybrid scheme, and GNSS are shown in Fig. 11. The zoomed plot on right side of the Fig. 11 shows that the pure INS velocities are drifted by 1m/sec and 0.5 m/sec (north and east channels) after 3500 sec whereas the errors in hybrid computed velocities are found to be < 0.05 m/sec and having close match with GNSS measured velocities.

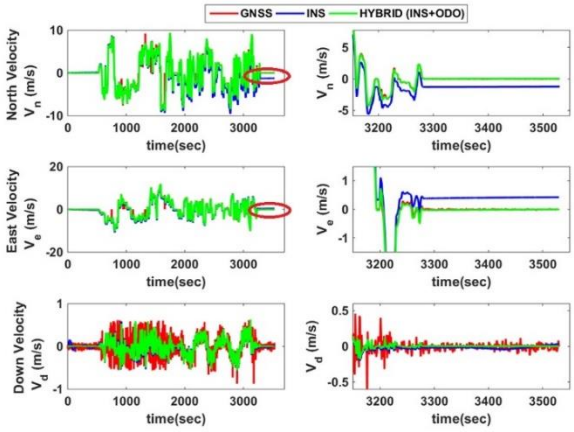

Fig. 11. Velocity profile of vehicle during motion testing

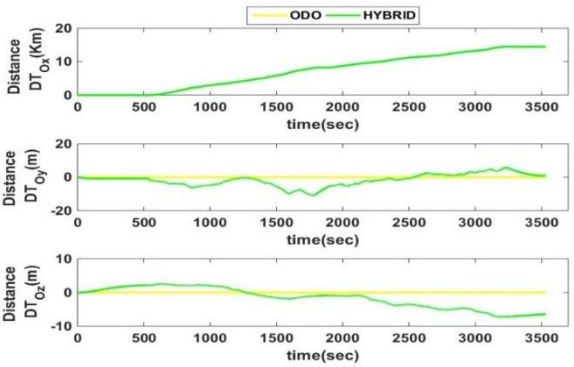

Fig. 12. Distance Travelled (DT) in odometer sensor body frame as shown by Hybrid Navigation mechanization and Odometer

The distance travelled (DT) information is presented in Fig. 12. It is found that the NHC constraints imposed on EKF process are very effective and distance computed along lateral DT_y and vertical axes DT_z are found to be less than 20 meters.

The estimated bias vectors of the gyroscopes and accelerometers are shown in Fig. 13. The gyro biases are found to be <0.03 deg/hour which are within the sensor specifications as shown Table. 1. Similarly, the accelerometers biases estimated to be around 70 µg which are within the sensor specifications as shown Table. 1.

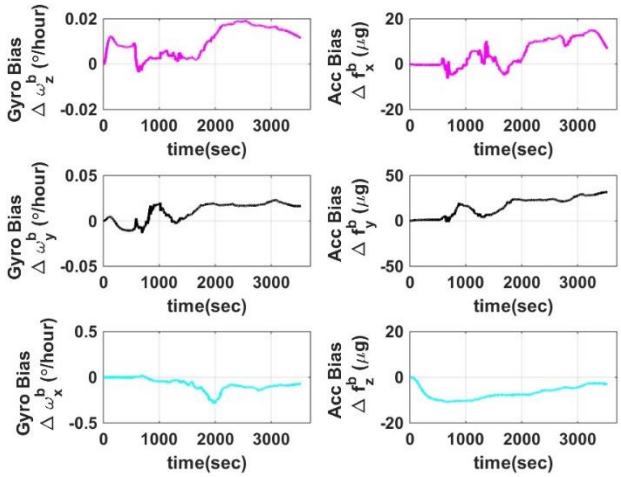

Fig. 13. Estimated biases of gyroscopes and accelerometer by Hybrid (INS+ODO) navigation mechanization

As discussed in the introduction part of manuscript, the estimability of proposed EKF with 21-states can be better judged by observing the estimated values of lever arm vector, scale factor and mis-alignment angles of odometer. Hence, the respective estimated parameters are plotted in Fig. 14. The estimated lever arm values for L_x and L_y are converged towards calibrated values within 200 sec from the start of vehicle.

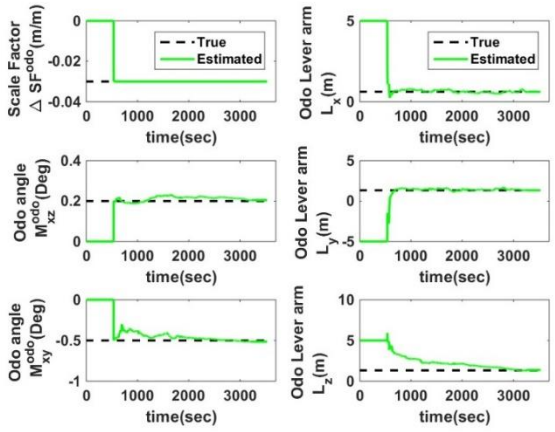

Fig.14. Estimated Odometer mis-alignment angles and lever arm states of Hybrid (INS+ODO) navigation mechanization

However, the convergence of vertical axis lever arm L_z is slower and took around 3000 sec. This is due to lower degree of observability for L_z. The van is kept static initially for a duration of 500 sec. During these static conditions the estimated scale factor did not see any corrections from EKF process. As soon as the vehicle started moving after 500 seconds, the scale factor is estimated immediately within few seconds and converged to pre-calibrated true value. The estimated mis-alignment angles are found to be converging within few seconds from the time of vehicle movement. But, these estimated angles have shown oscillatory behaviour. This is due to variations in measured and estimated velocities during vehicle rotations around the z_b axes.

Finally, it is important to express the positioning errors of proposed hybrid navigation scheme in terms of percentage of distance travelled. For a 15km distance, the errors found to be 0.2 % of DT and is shown in Fig. 15.

The error covariance of estimated state vectors are shown in Fig.16, Fig.17 and Fig.18. It is found the error covariance of horizontal positions ϕ_p and Θ_p are slowly diverging as expected due to no observability on horizontal position channels.

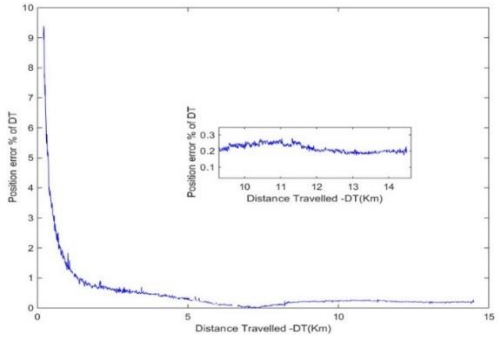

Fig.15. Positioning error proposed Hybrid navigation mechanization expressed as \% of Distance Travelled (DT)

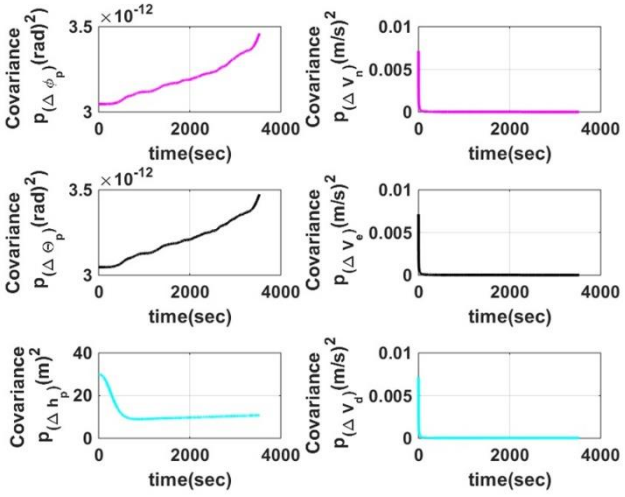

Fig.16. Covariance of error in position and velocity vectors of proposed Hybrid navigation with sequential EKF

However, the error covariance for vertical channel (height computation) has converged initially and remain stable for longer duration with a slow drift rate. This indicates that the error in height is successfully damped out. The error covariance of velocity vectors are converged quickly as it has high degree of observability as shown in Fig. 16.

The error covariance of augmented state vectors of odometer sensor assembly are shown in Fig.17. The convergence rate of respective error state vectors shown in Fig.14 has high level of correlation with respective error covariance as shown Fig. 17. Finally, the error covariance of attitude vectors, accelerometer bias vectors and gyro bias vectors are shown in Fig. 18 and found to be very much consistent with corresponding error state vectors shown in Fig.13.

The implementation details of fusion of inertial sensor data with odometer data has been described. Van trials are carried out to validate the proposed scheme and the associated sequential EKF algorithms along with non-holonomic constraints. The filed evaluation results of position error when odometer data is fused are compared with the position when GNSS feed is available. Hence, it is shown that a navigation system with the proposed hybrid navigation mechanization feature, can give high position accuracy even in GNSS non-available conditions.

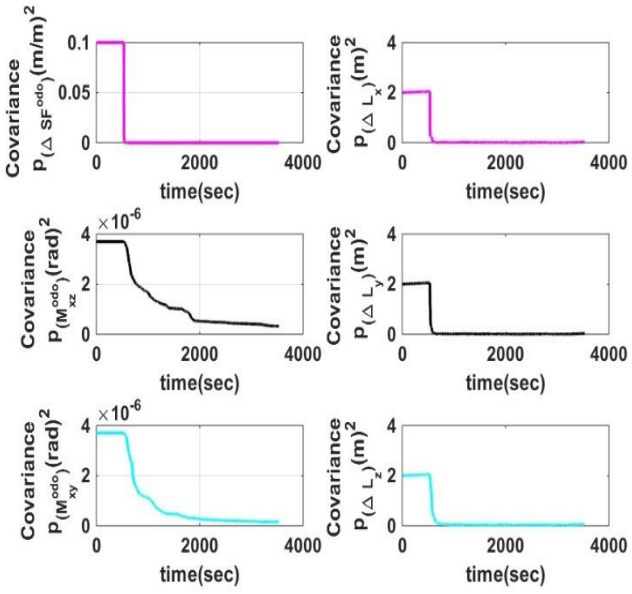

Fig. 17. Covariance of error in estimated Odometer mis-alignment angles and lever arm states of proposed Hybrid (INS+ODO) navigation mechanization with sequential EKF.

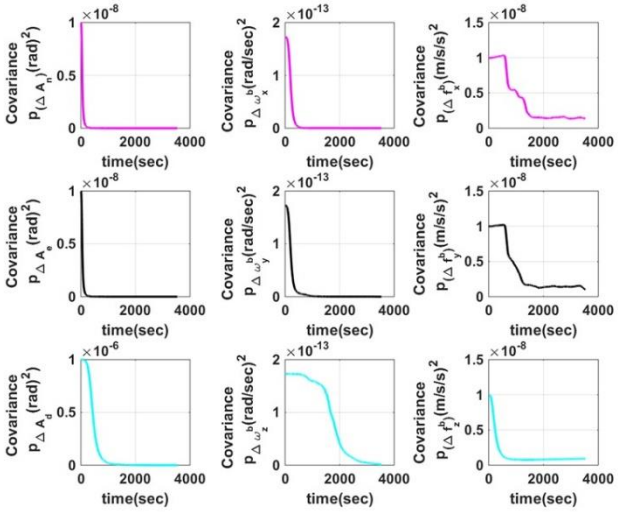

Fig. 18 Covariance of error in estimated attitude, gyro bias and accelerometer bias states of proposed Hybrid (INS+ODO) navigation mechanization with sequential EKF

6. CONCLUSION

In this manuscript, a 21-state EKF based hybrid navigation mechanization has been presented to have the high accuracy navigation solution for land vehicle applications. The mis-alignment angles and odometer scale factor errors are estimated and their accuracy is seen to be on par with calibrated values. Hence, the need of laborious calibration can be supplemented with proposed estimation process directly in the field. The method of pre-processing of odometer pulse measurements are considered and investigated for the positioning accuracy of SINS. The sequential processing of these measurements is considered for the proposed EKF. The field trial for 15km distanced travelled has demonstrated the improved performance as compared to traditional pure INS solution and could damp out the Schuler oscillations involved in horizontal channels of Pure INS mechanization. The work presented in the manuscript demonstrated the deployment of odometer as auxiliary sensor in tandem with SINS under GNSS outage conditions and enables the land vehicle to achieve the higher positioning accuracies as compared to stand alone operation of SINS.

Finally, it is evolved that the odometer can be a potential auxiliary sensor along with SINS towards multi-sensor data fusion for along with its superior performance for positioning application of autonomous vehicle under GNSS non-available conditions.

Acknowledgements

We are thankful to Dr. Anindya Bishwas, Director, RCI, Hyderabad for his motivation and support for taking up present research work.

Conflicts of interest

The authors declare no conflicts of interest.

References

[1] B. Lee, Y.J. Lee, and S. Sung, "An Efficient Integrated Attitude Determination Method Using Partially Available Doppler Measurement Under Weak GPS Environment," *Int. J. Control Autom. Syst.,* 16, pp. 3000–3012, 2018, https://doi.org/10.1007/s12555-017-0499-y

[2] S. Taghizadeh, and R. Safabakhsh, "An integrated INS/GNSS system with an attention-based hierarchical LSTM during GNSS outage," *GPS Solut.*, vol. 27, no. 71, 2023, https://doi.org/10.1007/s10291-023-01412-w

[3] K. Zhu, C. Deng, F. Zhang, H. Kang, Z. Wen and G. Guo, "A Multi-Source Fusion Navigation System to Overcome GPS Interruption of Unmanned Ground Vehicles," *IEEE Access*, vol. 11, pp. 61070-61081, 2023, doi: 10.1109/ACCESS.2023.3282219.

[4] Krishna Samalla and P.Naveen Kumar, "Investigation of Suitable Anti Spoofing Algorithm for GNSS Receivers," *International Journal of Intelligent Systems and Applications in Engineering*, *IJISAE*, vol. 12, no.4, pp. 373–377, 2024

[5] K.W. Chiang, H.W. Chang, Y.H. Li, G.J. Tsai, C.L. Tseng, Y.C. Tien, and P. C. Hsu, "Assessment for INS/GNSS/ Odometer/Barometer Integration in Loosely-Coupled and Tightly-Coupled Scheme in a GNSS-Degraded Environment," *IEEE Sens. J.*, vol. 20, no. 6, pp. 3057-3069, March15, 2020, doi:10.1109/JSEN.2019.2954532.

[6] J.G. Jungi Park, D.S. Lee and C. Park, "Implementation of Vehicle Navigation System using GNSS, INS, Odometer and Barometer," *J. Positioning, Navigation and Timing*, JPNT 4(3), pp. 141-150, 2015, doi:10.11003/JPNT.2015.4.3.141.

[7] S. A. chütz, D. E. Sánchez-Morales, and T. Pany, "Precise positioning through a loosely-coupled sensor fusion of GNSS-RTK, INS and LiDAR for autonomous driving," 2020 IEEE/ION Position, Location and Navigation Symp. (PLANS), Portland, OR, USA, 2020, pp. 219-225, doi: 10.1109/PLANS46316.2020.9109934.

[8] M. Wang, W. Wu, X. He, Y. Li, and X. Pan, "Consistent ST-EKF for Long Distance Land Vehicle Navigation Based on SINS/OD Integration," *IEEE Trans. on Vehicular Technol.*, vol. 68, no. 11, pp. 10525-10534, Nov, 2019. doi: 10.1109/TVT.2019.2939679.

[9] M. Zhong, J. Guo, and Z. Yang, "On Real-Time Performance Evaluation of the Inertial Sensors for INS/GPS Integrated Systems," *IEEE Sens. J.*, vol. 16, no. 17, pp. 6652-6661, Sept.1, 2016, doi: 10.1109/JSEN.2016.2588140.

[10] G. Dissanayake, S. Sukkarieh, E. Nebot, and H. Durrant-Whyte, "The aiding of a low-cost strap-down inertial measurement unit using vehicle model constraints for land vehicle applications*", IEEE Trans. Robot. Autom.*, vol.17, no.5, pp. 731–747, Oct. 2001, doi: 10.1109/70.964672.

[11] Y. Wu, M. Wu, X. Hu and D. Hu, "Self-calibration for Land Navigation Using Inertial Sensors and Odometer: Observability Analysis," *AIAA GNC Conference*, 10 - 13 August 2009, Chicago, Illinois, doi:10.2514/6.2009-5970.

[12] N. Vasilyuk, and D. Tokarev, "Identification of geometric displacements of odometers in a GNSS/inertial navigation system installed on a land vehicle," 2020 IEEE/ION PLANS, Portland, OR, USA, 2020, pp. 197-207, doi: 10.1109/PLANS46316.2020.9110193.

[13] L. Wang, X. Niu, T. Zhang, H. Tang, and Q. Chen, "Accuracy and robustness of ODO/NHC measurement models for wheeled robot positioning," *Meas.*, vol. 201, 2022, pp. 111720, https://doi.org/10.1016/j.measurement.2022.111720.

[14] S. Han, X. Ren, J. Lu and J. Dong, "An Orientation Navigation Approach Based on INS and Odometer Integration for Underground Unmanned Excavating Machine," *IEEE Transactions on Vehicular Technology*, vol. 69, no. 10, pp. 10772-10786, Oct. 2020, doi: 10.1109/TVT.2020.3010979

[15] Y. Wu, X. Niu and J. Kuang, "A Comparison of Three Measurement Models for the Wheel-Mounted MEMS IMU-Based Dead Reckoning System," *IEEE Transactions on Vehicular Technology*, vol. 70, no. 11, pp. 11193-11203, Nov. 2021, doi: 10.1109/TVT.2021.3102409

[16] L. Han, Z. Shi, J. Song and H. Wang, "Vehicle Positioning Algorithm Based on NHC/Virtual-MINS/OD," *IEEE Transactions on Vehicular Technology*, vol. 71, no. 5, pp. 4764-4775, May 2022, doi: 10.1109/TVT.2022.3157744

[17] H. Hu, K. Li, W. Liang, Q. Li and Z. Xie, "Kilometer Sign Positioning-Aided INS/Odometer Integration for Land Vehicle Autonomous Navigation," *IEEE Sensors Journal*, vol. 23, no. 4, pp. 4143-4158, 15 Feb.15, 2023, doi: 10.1109/JSEN.2023.3236063

[18] Q. Fu, Y. Liu, Z. Liu, S. Li and B. Guan, "High-Accuracy SINS/LDV Integration for Long-Distance Land Navigation," *IEEE/ASME Transactions on*

Mechatronics, vol. 23, no. 6, pp. 2952-2962, Dec. 2018, doi: 10.1109/TMECH.2018.2875151

[19] M. Yan, Z. Wang and J. Zhang, "Online Calibration of Installation Errors of SINS/OD Integrated Navigation System Based on Improved NHC," *IEEE Sensors Journal*, vol. 22, no. 13, pp. 12602-12612, 1 July1, 2022, doi: 10.1109/JSEN.2022.3170707

[20] M. Wang, J. Cui, Y. Huang, W. Wu and X. Du, "Schmidt ST-EKF for Autonomous Land Vehicle SINS/ODO/LDV Integrated Navigation," *IEEE Transactions on Instrumentation and Measurement*, vol. 70, pp. 1-9, 2021, Art no. 8504909, doi: 10.1109/TIM.2021.3122530

[21] Y. Cui, S. Liu, J. Yao and C. Gu, "Integrated Positioning System of Unmanned Automatic Vehicle in Coal Mines," *IEEE Transactions on Instrumentation and Measurement*, vol. 70, pp. 1-13, 2021, Art no. 8503013, doi: 10.1109/TIM.2021.3083903

[22] B. Yang, L. Xue, H. Fan and X. Yang, "SINS/Odometer/Doppler Radar High-Precision Integrated Navigation Method for Land Vehicle," *IEEE Sensors Journal*, vol. 21, no. 13, pp. 15090-15100, 1 July1, 2021, doi: 10.1109/JSEN.2021.3071181

[23] X. Li, Z. Qin, Z. Shen, X. Li, Y. Zhou and B. Song, "A High-Precision Vehicle Navigation System Based on Tightly Coupled PPP-RTK/INS/Odometer Integration," *IEEE Transactions on Intelligent Transportation Systems*, vol. 24, no. 2, pp. 1855-1866, Feb. 2023, doi: 10.1109/TITS.2022.3219895.

[24] W. Gao, J. Li, G. Zhou, and Q. Li, "Adaptive Kalman Filtering with Recursive Noise Estimator for Integrated SINS/DVL Systems," *Journal of Navigation*, vol. 68, no. 1, pp. 142-161, 2015, doi:10.1017/S0373463314000484

[25] H. Zhao, L. Miao, and H. Shao, "Adaptive Two-stage Kalman Filter for SINS/Odometer Integrated Navigation Systems," *Journal of Navigation*, vol. 70, no. 2, pp. 242-261, 2017, doi:10.1017/S0373463316000485

[26] He Chen, Zhang Zhili, Zhaofa Zhou, Pengpeng Liu, and Qi Guo, "SINS/OD Integrated Navigation Algorithm Based on Body Frame Position Increment for Land Vehicles," *Mathematical Problems in Engineering*, 5719472, 11 pages, 2018. https://doi.org/10.1155/2018/5719472

[27] A. Gelb, "Applied Optimal Estimation", Cambridge, MA: MIT Press, 1974

[28] Mohinder S Grewal, "Global Positioning Systems, Inertial Navigation and Integration", A John Wiley and Sons, Inc, Publications}, Second Edition, 2007.

[29] C. Yang, W. Shi, and W. Cheng, "Robust M–M unscented Kalman filtering for GPS/IMU navigation," *J. Geod.*, 93, pp. 1093–1104, 2019, https://doi.org/10.1007/s00190-018-01227-5

[30] C. Yang, W. Shi, and W. Chen, "Comparison of Unscented and Extended Kalman Filters with Application in Vehicle Navigation," *Journal of Navigation*, vol. 70, no. 2, pp. 411-431, 2017. doi:10.1017/S0373463316000655

[31] J. N. Gross, Y. Gu, M. B. Rhudy, S. Gururajan and M. R. Napolitano, "Flight-Test Evaluation of Sensor Fusion Algorithms for Attitude Estimation," *IEEE Transactions on Aerospace and Electronic Systems*, vol. 48, no. 3, pp. 2128-2139, JULY 2012, doi: 10.1109/TAES.2012.6237583